**Table 1 Molecular characteristics of polymers**

| Polymer | $M_w$ | Polydispersity index |
|---|---|---|
| PS | 94.9 K | 1.06 |
| PVP | 115 K | 1.03 |
| PSBr | 215 K | 1.02 |

$M_w$, weight average molecular weight. All materials were used as obtained from the Polymer Standards Service (Mainz, Germany). The degree of bromination of the PSBr was 52.2 mol %.

thermodynamic equilibrium. The rectangular cross-section of the PS phase in Fig. 2c is a direct consequence of this rapid solidification of the binary polymer blend[6]. In contrast, wetting experiments of a single liquid on a patterned substrate show a more rounded topography[8].

These results were achieved only after careful optimization of several experimental parameters. For a given pattern periodicity, perfect lateral organization of the polymer phases is observed only for a given film thickness. To explore the optimum conditions for the self-organization process and to demonstrate the universality of our approach, a second binary polymer mixture on a different prestructured substrate surface was investigated. Mixtures of PS and a partially brominated polystyrene (PSBr) were spun-cast onto patterned silicon oxide ($SiO_x$)/hydrogen-terminated silicon (SiH) surfaces with varying grating periodicities. AFM cross-sections of the as-cast films and of the remaining PSBr phases after removing the PS (data not shown) are superimposed to yield the cross-sectional domain morphologies. In Fig. 3a, b a partial surface directed reorganization of PSBr and PS domains has taken place, but the lateral organization is incomplete. Figure 3a, b reveals a phase behaviour that is very similar to the separation of a PS/PSBr mixture on homogeneous $SiO_x$ and SiH surfaces, respectively: PS/PSBr bilayers on the SiH surface regions and a lateral PS/PSBr phase morphology with ~1-μm-wide PSBr domains surrounded by the PS phase on $SiO_x$. As the film thickness is increased, the quality of the pattern replication successively improves (Fig. 3c, d). For a given film thickness (that is, 65 nm in Fig. 3a), on the other hand, a reduction of the substrate periodicity leads to a better lateral order of the domain morphology (Fig. 3e, f). The results shown in Fig. 3 suggest an underlying principle that governs the ordering process. We compared the ~1 μm average size of the PSBr domains on the $SiO_x$ surface regions in Fig. 3a with the 750-nm stripe width of the SiH/$SiO_x$ substrate pattern in Fig. 3e: this indicated that complete ordering of the polymer phases can occur only for pattern sizes comparable to the characteristic length of the lateral domain morphology on the respective homogeneous substrate. Although the details of the surface-induced demixing process are not yet known, the existence of a well defined lateral length scale suggests a bulk- or surface spinodal instability which develops during the spin-coating process. A quantitative study of phase separation during spin-coating is currently underway.

We have made use of two fundamental thermodynamic principles—phase separation of a binary fluid and selective adsorption from a binary mixture—to transpose a variation in surface energies of a flat substrate into a concentration variation of a binary polymer film. The micrometre size structures perfectly replicate the substrate pattern over lateral dimensions which are limited only by the sample size (1 $cm^2$ in our case). The size of the structures that can be produced is at present dictated by the availability of substrate templates, and lateral structure sizes of less than 100 nm should be feasible. We emphasize that the structures reported here are replicated from a prepatterned substrate, rather than driven by a molecular self-organization process, as for example in microphase separated block-copolymer melts[9]. In these systems, the morphology of the lateral structure is determined by the architecture of the constituent molecules, and long-range order is difficult to achieve[10]. But with our approach, a given experimental system (that is, a particular polymer blend) can be used to produce structures of widely varying morphologies and length scales. In contrast to bare patterned SAM substrates, the patterned polymer films are thick enough to allow further semiconductor processing steps such as reactive ion etching. Moreover, the polymer layers can be lifted off the substrates, and several structured films can be superimposed. Therefore, patterned SAM surfaces can be used as templates for multiple pattern replication. We also note that the manufacture of the structured polymer films takes just a few minutes, is inexpensive, and, once optimized, is highly reproducible. From a technological viewpoint, various applications can be envisaged, such as the formation of photonic bandgap materials[11], patterned polymer surfaces with selective molecular recognition capabilities[12], and optical devices[13]. In addition to their technological relevance, lateral nanoscale structures in polymer films could provide a new tool to study phase equilibria near surfaces on a molecular level. □

Received 19 September; accepted 9 December 1997.

1. Gunton, J. D., San Miguel, M. & Sahni, P. S. in *Phase Transitions and Critical Phenomena* (eds Domb, C. & Lebovitz, J. L.) Vol. 8, 267–466 (Academic, London, 1983).
2. Jones, R. A. L., Norton, L. J., Kramer, E. J., Bates, F. S. & Wiltzius, P. Surface-directed spinodal decomposition. *Phys. Rev. Lett.* **66,** 1326–1329 (1991).
3. Krausch, G., Kramer, E. J., Rafailovich, M. H. & Sokolov, J. Self assembly of a homopolymer mixture via phase separation. *Appl. Phys. Lett.* **64,** 2655–2657 (1994).
4. Xia, Y., Zaho, X.-M. & Whitesides, G. M. Pattern transfer: Self-assembled monolayers as ultrathin resists. *Microelectr. Eng.* **32,** 255–268 (1996).
5. Service, R. F. Patterning electronics on the cheap. *Science* **278,** 383–384 (1997).
6. Walheim, S., Böltau, M., Mlynek, J., Krausch, G. & Steiner, U. Structure formation via polymer demixing in spin-cast films. *Macromolecules* **30,** 4995–5003 (1997).
7. Binning, G., Quate, C. F. & Gerber, C. Atomic force microscope. *Phys. Rev. Lett.* **56,** 930–933 (1986).
8. Abbot, N. L., Folkers, J. P. & Whitesides, G. M. Manipulation of the wettability of surfaces on the 0.1- to 1-micrometer scale through micromachining and molecular self assembly. *Science* **257,** 1380–1382 (1992).
9. Morkved, T. L., Wiltzius, P., Jaeger, H. M., Grier, D. G. & Witten, T. A. Mesoscopic self-assembly of gold islands on diblock-copolymer films. *Appl. Phys. Lett.* **64,** 422–424 (1994).
10. Morkved, T. L. *et al.* Local control of microdomain orientation in diblock copolymer thin films with electric fields. *Science* **273,** 931–933 (1996).
11. Haus, J. W. in *Quantum Optics of Confined Systems* (eds Ducloy, M. & Block, D.) 101–141 (Kluwer Academic, Dordrecht, 1996).
12. Prime, K. L. & Whitesides, G. M. Self-assembled organic monolayers: Model systems for studying adsorption of proteins at surfaces. *Science* **252,** 1164–1167 (1991).
13. Halls, J. *et al.* Efficient photodiodes from interpenetrating networks. *Nature* **376,** 498–500 (1995).

**Acknowledgements.** This work was supported by the Deutsche Forschungsgesellschaft (DFG), the Volkswagenstiftung, and NATO. U.S. acknowledges the financial support from a research fellowship (Habilitations-Stipendum) of the DFG. We thank E. J. Kramer and J. Heier for their help preparing the PDMS stamps.

Correspondence and requests for materials should be addressed to U.S. (e-mail address: Ulli.Steiner@uni-konstanz.de).

# Origin of upper-ocean warming and El Niño change on decadal scales in the tropical Pacific Ocean

**Rong-Hua Zhang*, Lewis M. Rothstein* & Antonio J. Busalacchi†**

* *Graduate School of Oceanography, University of Rhode Island, Narragansett, Rhode Island 02882, USA*

† *Laboratory for Hydrospheric Process, NASA Goddard Space Flight Center, Greenbelt, Maryland 20771, USA*

**The cause of decadal-scale variability in the tropical Pacific Ocean—such as that marked by the 1976–77 shift in the El Niño/Southern Oscillation[1–7]—is poorly understood. Unravelling the mechanism of the recent decade-long warming in the tropical upper ocean is a particularly important challenge, given the link to El Niño variability, but establishing the hypothesized inter-annual/decadal oceanic connections between middle latitudes and tropics has proved elusive[8]. Here we present observational evidence that Pacific upper-ocean warming and decadal changes in the El Niño/Southern Oscillation after 1976 may originate from**

**decadal mid-latitude variability. In the middle 1970s the North Pacific Ocean is observed to have undergone a clear phase-transition; a 'see-saw' subsurface temperature anomaly pattern that rotates clockwise around the subtropical gyre. At middle latitudes a subsurface warm anomaly formed in the early 1970s from subducted surface-waters and penetrated through the subtropics and into the tropics, thus perturbing the tropical thermocline and driving the formation of a warm surface-water anomaly that may have influenced El Niño in the 1980s. The identification of this teleconnection of extratropical thermal anomalies to the tropics, through a subsurface ocean 'bridge', may enable improved prediction of decadal-scale climate variability.**

We have examined recently available observations[9–12] of the Pacific basin, looking for interrelationships between the extratropics and tropics on interannual and interdecadal scales. Atmospheric variables were obtained from a new analysis of surface marine anomalies derived from the Comprehensive Ocean–Atmosphere Data Sets (COADS) from January 1945 to December 1989[13]. The oceanic data were yearly *in situ* temperature anomalies at 13 standard levels from the sea surface to 400 m depth analysed by Levitus *et al.*[9] The yearly anomaly fields were produced by subtracting

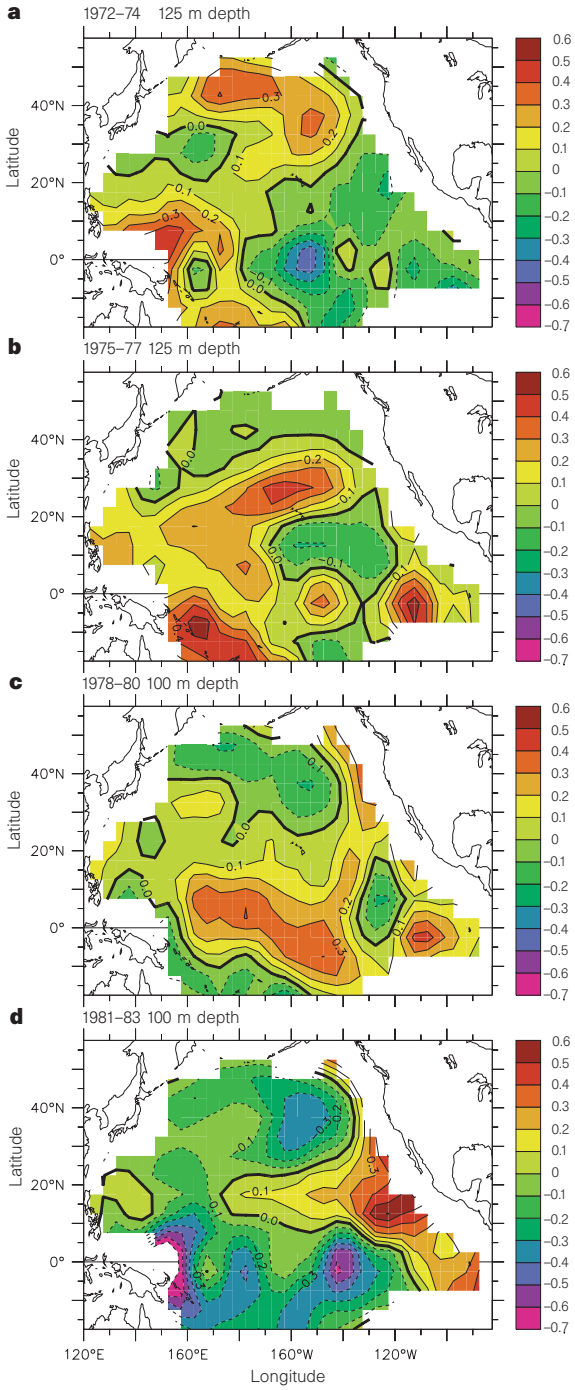


**Figure 1** Horizontal distribution of ocean temperature anomalies averaged for four consecutive 3-year periods. Temperatures were measured at either 125 m depth (**a**, 1972–74; **b**, 1975–77) or at 100 m depth (**c**, 1978–80; **d**, 1981–83). The choice of different depths for detecting the basin-scale anomaly patterns of interest reflects the fact that the thermocline in the tropics is shallower than at middle latitudes. We note that some subsurface warm anomalies have penetrated from the middle latitudes into the tropics in **a** and **b**, and can be seen to extend eastwards in the tropics in **c** and **d**. The contour interval is 0.1 °C, with the colour bar on the right indicating anomalies from –0.7 to 0.6 °C.

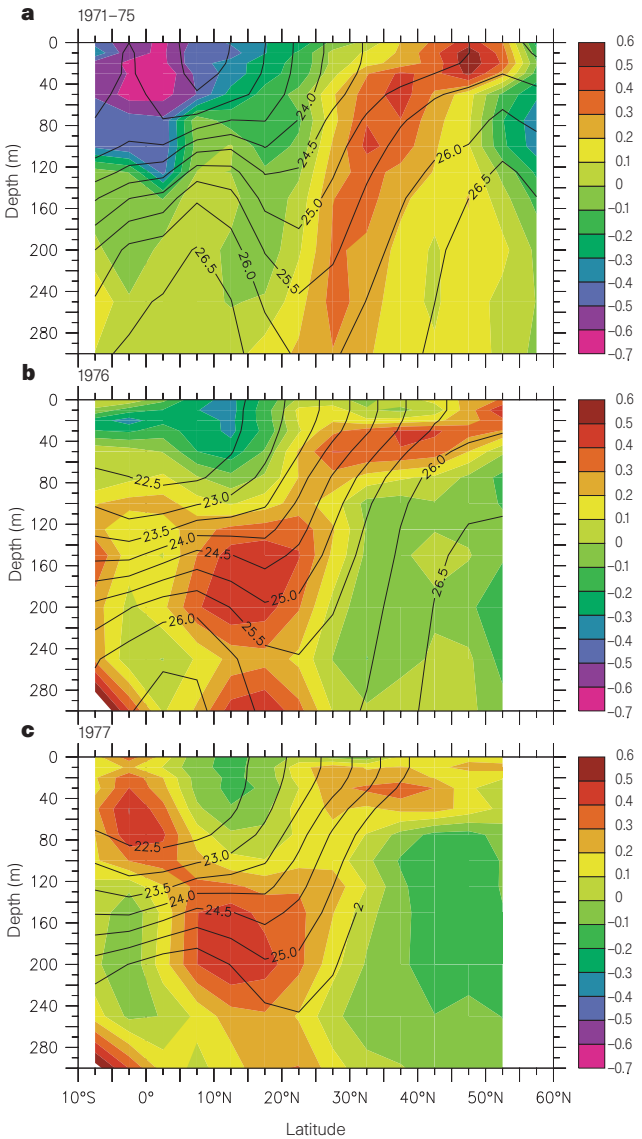


**Figure 2** Meridional-depth sections of upper-ocean temperature anomalies (colour) and isopycnal surfaces (kg m$^{-3}$; contour lines). Sections are along 157.5° W for years 1971–75 (**a**), and along 177.5° E for years 1976 (**b**) and 1977 (**c**). Two different longitudinal sections have been used to show clearly the signals of interest (for example, the warm anomaly subduction occurs mainly in the eastern North Pacific whereas the warm anomaly penetration from the subtropics into tropics occurs in the central basin). The colour bar on the right indicates temperature anomalies from –0.7 to 0.6 °C with intervals of 0.1 °C.

the averaged values from the 1961–90 mean values for the ocean, and from the 1961–89 mean values for the atmosphere.

To examine the spatial structure of decadal variability over the entire Pacific, we put together atmospheric and oceanic anomaly fields for three periods: from 1965 to 1972, from 1975 to 1977, and from 1980 to 1988. The choice of these averaged time periods is based on previous empirical orthogonal function (EOF) analyses of upper-ocean temperature anomalies as best representing the decadal warm and cold phases in the North Pacific, and their transition during 1975–77[12]. During the period 1965–72, that is, the decadal warm phase (relative to the central middle latitudes), the Aleutian Low weakens, accompanied by anomalous anticyclonic circulation over the North Pacific, with easterly wind anomalies prevailing in the western tropical basin. Sea surface temperature (SST) is anomalously warm over the eastern and central middle latitudes, but is cold off the west coast of North America and in the tropical and subtropical regions. An abrupt shift of SST and atmospheric circulation occurs late in 1976[1–6], characterized by, among other things, a warming through much of the tropical central and eastern Pacific Ocean.

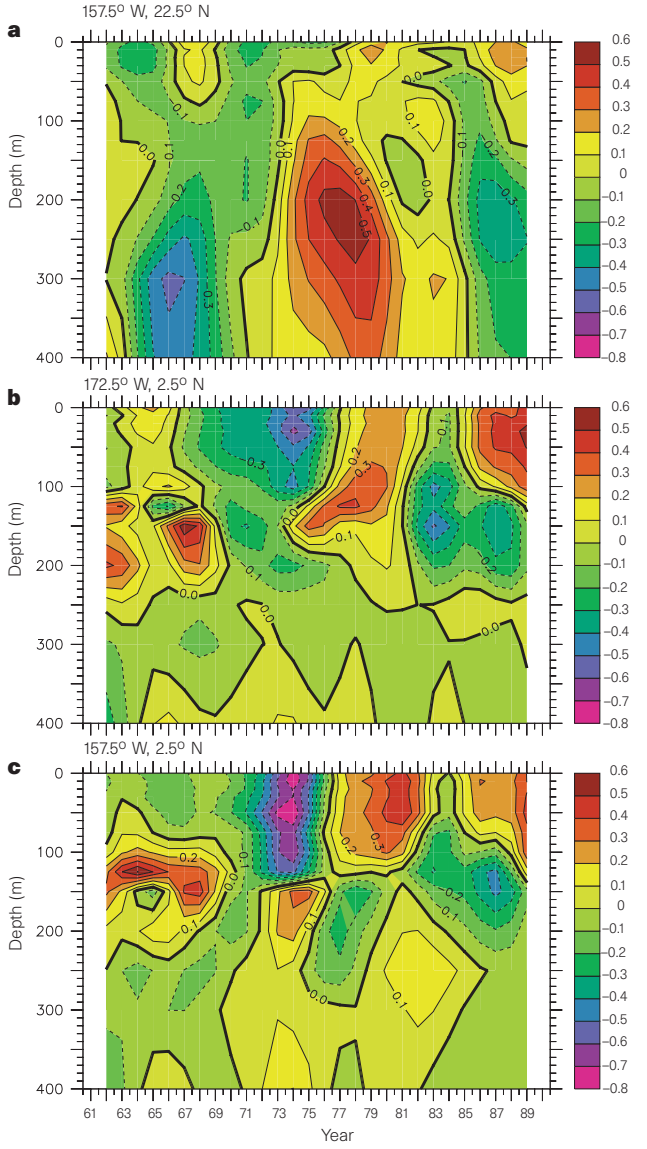


**Figure 3** Upper ocean temperature anomalies as a function of depth and time in different locations. **a**, At 157.5° W and 22.5° N; **b**, at 172.5° W and 2.5° N; **c**, at 157.5° W and 2.5° N. A three-year running-mean filter has been applied to these data. The contour interval is 0.1 °C with the colour bar on the right indicating anomalies from –0.8 to 0.6 °C.

The upper-ocean temperature data set[9] enables us to investigate the oceanographic component of this decadal variability over the entire Pacific; its basin-scale structure and evolution has been recently documented[9,11,12]. Figure 1 shows the time-averaged temperature anomalies at subsurface depths in the sequence of four time periods. There is a well-defined pattern and an orderly space-time evolution around the subtropical gyre, with prominent planetary wave signatures in the subtropics[12,14–16]. These features have been more clearly detected from EOF and regression pattern analyses[12]. During the pre-1976–77 period, for about a decade, a large subsurface warm temperature anomaly covers the central middle latitudes, with cold anomalies in the subtropics (Fig. 1a). During the period 1976–77 (Fig. 1b), an apparent reversal of anomaly polarity begins to occur: the warm mid-latitude anomaly circulates southwestwards in the eastern subtropics while at the same time penetrating into the western subtropics and tropics, where there is also a corresponding warming. These subsurface anomalies continue to evolve on the basin scale (Fig. 1c, d).

The observed subsurface thermal anomalies tend to persist as they move around the basin and can be transported to the sea surface within strong upwelling and/or vertical mixing regions such as in the equatorial Pacific. The subsurface warm anomalies observed to have subducted in the middle latitudes in the late 1960s and early 1970s may therefore serve as the origin of upper-ocean warming (and decadal climate change) in the tropical Pacific in the 1980s.

In Figs 2–4 we show the chronological evidence for connections between surface and subsurface temperature anomalies at middle latitudes and in the tropics. Mid-latitude air–sea interactions produce persistent warm anomalies at the sea surface that are subducted into the thermocline (Fig. 2a) and then move westward and equatorward around the subtropical gyre on isopycnal surfaces[10,17]. The subducted North Pacific thermocline warm anomaly, observed first at middle latitudes in the late 1960s and early 1970s, starts to circulate toward the Equator at subsurface ocean depths. In the middle 1970s, a strong warm anomaly has detached from the surface and is found in the central subtropics at depth (Fig. 3a).

Subsurface midlatitude-to-tropical ocean connections are further demonstrated in Fig. 4. During the 1960s and until about 1974, temperature variations are out of phase in the middle latitudes and tropics: a warm anomaly in the north, and a mainly cold anomaly to the south (Fig. 4a, b). Such out-of-phase variations are also evident during the 1980s, but with opposite sign. Throughout the 1970s and early 1980s, a slow southward propagation of a warm anomaly can be seen from the middle latitudes through the subtropics and into tropics (Fig. 4c). By the early 1970s, a related subsurface warm anomaly has already occurred in the far western tropical Pacific (Fig. 1a). However, a clear incursion of the extratropical warm anomaly into the tropics takes place in the middle 1970s (Fig. 2b, c).

We show the links between tropical subsurface and surface temperature anomalies in Fig. 2b, c and Fig. 3b, c, respectively. In 1976 (Fig. 2b), the largest warm anomaly (+0.4 °C) is located at 140–220 m depth between 8° N and 23° N in the central Pacific, with cold surface anomalies in the tropics. For the year 1977, the three-dimensional structure of temperature anomalies in a depth–latitude section can be seen in Fig. 2c. A significant warm anomaly is centred at ~180 m depth in the off-equatorial region (at ~13° N). Having become detached from the chief off-equatorial warm-anomaly centre, another warm anomaly can be seen to form in the equatorial region at relatively shallow depths (at ~70 m) in the central Pacific. The time–depth evolution is shown in Fig. 3b. A tail structure is clearly evident, with a warm anomaly originating from subsurface depths and spreading upwards with time. Based on our more complete and detailed analyses (not shown), the shallow equatorial warm anomaly is most likely to have come from the North Pacific subtropics, with anomalies at the sea surface lagging those at depth and to the west on the Equator. This anomaly seems

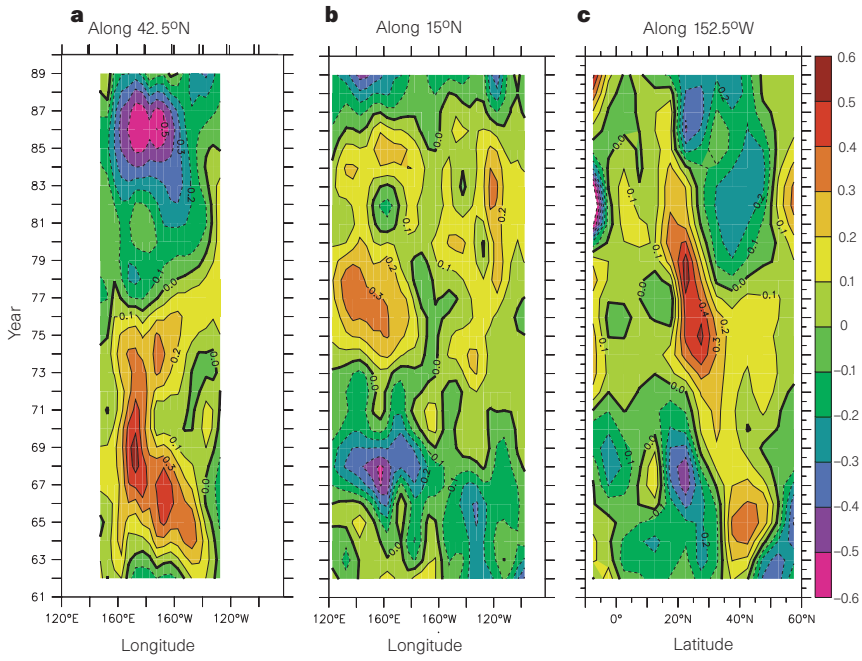


**Figure 4** Ocean temperature variations with time from 1960 to 1990 at 250 m depth. The data are plotted against longitude along 42.5° N (**a**), against longitude along 15° N (**b**), and against latitude along 152.5° W (**c**), demonstrating subsurface connections between temperature anomalies at middle latitudes and in the tropics. The contour interval is 0.1 °C, with dashed lines for cold anomalies. A three-year running mean filter has been applied to these data.

to be responsible for changes in the background thermal state and the behaviour of El Niño/Southern Oscillation (ENSO) immediately after 1976. Indeed, on the Equator, clear phase relationships between decadal anomalies of subsurface temperature and SST have been reported[11], with subsurface warm anomalies in the west preceding large-scale surface warming to the east. Further data analyses (not shown) indicate that decadal subsurface temperature variability in the tropics is not simply forced by tropical surface wind anomalies, which, in fact, are largely a response to SST changes. In addition, the subsurface warm anomalies appear to extend eastward along the Equator (Fig. 1b, c and Fig. 3b, c) and continue to move northward along the eastern boundary and, subsequently, westward away from the boundary in the subtropics as observed in the early 1980s (Fig. 1d).

So there are links between extratropical and tropical temperature anomalies through a subsurface ocean 'bridge' for the middle and late 1970s. The decadal warm-anomaly incursion from mid-latitude subduction sites into the tropics seems to form a warm thermocline anomaly in the western and central tropics. Once the tropical subsurface thermal structure has been perturbed, modelling studies have demonstrated how this temperature anomaly at depth can be communicated to the surface to influence SST in regions of strong vertical mixing and upwelling[18,19]. Thus the extratropical warm anomaly may induce upper-ocean warming in the central and eastern tropics, which, in turn, can produce surface westerly wind anomalies to the west, setting up air–sea interactions. This helps to explain the observed decadal-scale ENSO variability in the 1980s, that is, the extremely strong 1982–83 ENSO, and the frequent occurrence of the El Niño warm phase but a lack of a cold phase.

These findings reported here have significant implications from a variety of perspectives. Many low-frequency climate signals have been ascribed to El Niño in the tropics, while the role of the mid-latitude ocean has been less studied. In particular, the 1976–77 Pacific climate shift in the middle and high latitudes has been explained as a decadal effect of tropical interannual variations[1,4–6]. In fact, variations in the tropical Pacific are dominated by interannual signals[20]; there are no potential mechanisms or processes which have been identified that could maintain a self-sustained tropical decadal oscillation. This suggests that observed decadal tropical variability may be better traced to decadal extratropical processes. As demonstrated here, before the tropical warming in the middle and late 1970s, a decadal transition from a warm to cold phase occurs first in the North Pacific. Thus, thermocline anomalies associated with mid-latitude subduction processes may play an important role in perturbing tropical low frequency variability.

Our work also provides a basinwide, observational perspective on Pacific climate variability which suggests that temperature anomalies associated with the mid-latitude thermocline variability can penetrate all the way into the tropics. This is consistent with recent model studies of water pathways in the subtropical-tropical Pacific Ocean[21–23]. Identification of such anomaly patterns in the ocean, as well as in the atmosphere[24], is important for understanding and prediction of decadal climate variability. For example, recent modelling studies of ENSO predictability[25,26] have identified a decadal scale variability in prediction skill. It has been suggested that such changes may arise if there were changes to the background state of the tropical Pacific Ocean. Here we have seen a link between the middle latitudes and tropics that offers the potential of using the lead time intrinsic to the North Pacific subsurface thermal pattern to forecast decadal ENSO variability in the tropics.

The unusual warming in the tropical Pacific Ocean observed in the early 1990s[27,28] appears to be different from the warmings of the 1970s and 80s. It seems likely, for instance, that the propagation of cold extratropical anomalies (Fig. 4c) into the tropics in the late 1980s would introduce a cooling tendency in the tropical Pacific Ocean. The nature of the unexpected warming in the early 1990s has indeed been a topic of much debate[27,28]; is it a forced global warming signature or is it natural climate variability? Different decadal variability modes and the effects of the South Pacific Ocean are also possible. Sufficient temporal data coverage is not yet available to resolve these questions. □

Received 24 February; accepted 15 December 1997.

1. Trenberth, K. E. & Hurrell, J. W. Decadal atmosphere-ocean variations in the Pacific. *Clim. Dyn.* **9,** 303–319 (1994).
2. Ebbesmeyer, C. C. *et al.* in *Proc. 7th Ann. Pacific Climate Workshop* (Interagency Ecol. Stud. Prog. Rep. 26, Calif. Dept. of Water Resource, Los Angeles, 1991).
3. Nitta, T. & Yamada, S. Recent warming of tropical sea surface temperature and its relationship to the Northern Hemisphere circulation. *J. Meteorol. Soc. Jpn* **67,** 375–383 (1989).
4. Graham, N. E. Decadal scale variability in the tropical and North Pacific during the 1970s and 1980s: observations and model results. *Clim. Dyn.* **10,** 135–162 (1994).
5. Miller, A. J. *et al.* The 1976–77 climate shift of the Pacific Ocean. *Oceanography* **7,** 21–26 (1994).
6. Miller, A. J. *et al.* Interdecadal variability of the Pacific Ocean: model response to observed heat flux and wind stress anomalies. *Clim. Dyn.* **9,** 287–302 (1994).
7. Wang, B. Interdecadal changes in El Niño onset in the last four decades. *J. Clim.* **8,** 267–285 (1995).
8. Kerr, R. A. Unmasking a shifty climate system. *Science* **255,** 1508–1510 (1992).
9. Levitus, S., Boyer, T. P. & Antonov, J. *World Ocean Atlas* Vol. 5, *Interannual Variability of Upper Ocean Thermal Structure* (Atlas NESDIS 5, NOAA, Silver Spring, 1994).

10. Deser, C., Alexander, M. A. & Timlin, M. S. Upper ocean thermal variations in the North Pacific during 1970–1991. *J. Clim.* **9,** 1840–1855 (1996).
11. Zhang, R.-H. & Levitus, S. Structure and evolution of interannual variability of the tropical Pacific upper ocean temperature. *J. Geophys. Res.* **101,** 20501–20524 (1996).
12. Zhang, R.-H. & Levitus, S. Structure and cycle of decadal variability of upper ocean temperature in the North Pacific. *J. Clim.* **10,** 710–727 (1997).
13. Da Silva, M., Young, C. C. & Levitus, S. *Atlas of Surface Marine Anomalies* Vol. 2, *Directly Observed Quantities* (Atlas NESDIS 7, NOAA, Silver Spring, 1994).
14. Jacobs, G. A. *et al.* Decade-scale trans-Pacific propagation and warming effects of an El Niño anomaly. *Nature* **370,** 360–363 (1994).
15. Latif, M. & Barnett, T. P. Causes of decadal climate variability over the North Pacific and North America. *Science* **266,** 634–637 (1994).
16. Latif, M. & Barnett, T. P. Decadal climate variability over the North Pacific and North America: dynamics and predictability. *J. Clim.* **9,** 2407–2423 (1996).
17. Gu, D.-F. & Philander, S. G. H. Interdecadal climate fluctuations that depend on exchanges between the tropical and extratropics. *Science* **275,** 805–807 (1997).
18. Hirst, A. C. & Godfrey, J. S. The role of Indonesian throughflow in a global ocean GCM. *J. Phys. Oceanogr.* **23,** 1057–1086 (1993).
19. Liu, Z. & Philander, S. G. H. How different wind stress affect the tropical-subtropical circulations of the upper ocean. *J. Phys. Oceanogr.* **25,** 449–462 (1995).
20. Philander, S. G. H. *El Niño, La Niña and the Southern Oscillation* (Academic, New York, 1990).
21. Liu, Z. A simple model of the mass exchange between the subtropical and tropical ocean. *J. Phys. Oceanogr.* **24,** 1153–1165 (1994).
22. McCreary, J. P. & Lu, P. Interaction between the subtropical and equatorial ocean circulations: the subtropical cell. *J. Phys. Oceanogr.* **24,** 466–497 (1994).
23. Rothstein, L. M., Zhang, R.-H., Busalacchi, A. J. & Chen, D. A numerical simulation of the mean water pathways in the subtropical and tropical Pacific Ocean. *J. Phys. Oceanogr.* **28,** 322–342 (1998).
24. Bjerknes, J. Atmospheric teleconnections from the equatorial Pacific. *Mon. Weath. Rev.* **97,** 163–172 (1969).
25. Balmaseda, M. A., Davey, M. K. & Anderson, D. L. T. Decadal and seasonal dependence of ENSO prediction skill. *J. Clim.* **8,** 2705–2715 (1995).
26. Chen, D., Zebiak, S. E., Busalacchi, A. J. & Cane, M. A. An improved procedure for El Niño forecasting: Implications for predictability. *Science* **269,** 1699–1702 (1995).
27. Trenberth, K. & Hoar, T. The 1990–95 El Niño-South Oscillation event: Longest on record. *Geophys. Res. Lett.* **23,** 57–60 (1996).
28. Latif, M., Kleeman, R. & Eckert, C. Greenhouse warming, decadal variability, or El Niño? an attempt to understand the anomalous 1990s. *J. Clim.* **10,** 2221–2239 (1997).

**Acknowledgements.** We thank S. Levitus and other staff at the Ocean Climate Laboratory (NODC/NOAA) for their help and support in analysing observational data, and also thank M. Latif, Z. Liu, S. Tett, C. Deser, X.-Z. Liang and J. Picaut for comments. This work was supported by the NSF, NOAA and NASA.

Correspondence and requests for materials should be addressed to R.-H.Z. (e-mail address: zrh@sequan.gso.uri.edu).

# Evidence for pressure-release melting beneath magmatic arcs from basalt at Galunggung, Indonesia

**T. W. Sisson* & S. Bronto†**

* *US Geological Survey, 345 Middlefield Road, Menlo Park, California 94025, USA*

† *Volcanological Survey of Indonesia, Jl. Diponegoro no. 57, Bandung, 40122 Indonesia*

**The melting of peridotite in the mantle wedge above subduction zones is generally believed to involve hydrous fluids derived from the subducting slab[1]. But if mantle peridotite is upwelling within the wedge, melting due to pressure release could also contribute to magma production. Here we present measurements of the volatile content of primitive magmas from Galunggung volcano in the Indonesian arc which indicate that these magmas were derived from the pressure-release melting of hot mantle peridotite. The samples that we have analysed consist of mafic glass inclusions in high-magnesium basalts. The inclusions contain uniformly low $H_2O$ concentrations (0.21–0.38 wt%), yet relatively high levels of $CO_2$ (up to 750 p.p.m.) indicating that the low $H_2O$ concentrations are primary and not due to degassing of the magma. Results from previous anhydrous melting experiments on a chemically similar Aleutian basalts[2] indicate that the Galunggung high-magnesium basalts were last in equilibrium with peridotite at ~1,320 °C and 1.2 GPa. These high temperatures at shallow sub-crustal levels (about 300–600 °C hotter than predicted by geodynamic models[1,3]), combined with the production of nearly $H_2O$-free basaltic melts, provide strong evidence that pressure-release melting due to upwelling in the sub-arc mantle has taken place. Regional low-potassium[4] and low-$H_2O$ (ref. 5) basalts found in the Cascade arc indicate that such upwelling-induced melting can be widespread.**

Galunggung, an arc magmatic-front volcano in western Java, Indonesia, erupted in 1982–83 (ref. 6). Activity began with andesitic pyroclastic flows and products became more mafic with time, ending in several months of strombolian and effusive eruptions of high-Mg basalt (10.0–11.8 wt% MgO). These basalts have high concentrations of compatible trace elements[7], have compositions similar to Aleutian arc high-Mg basalts (Table 1), and carry phenocrysts of olivine to $Fo_{91}$ (although most are $Fo_{88}$; Fo = 100 Mg/(Mg + Fe)), as well as diopside, Cr-spinel and plagioclase. The primitive compositions of the high-Mg basalts, their primitive phenocrysts, and their mantle-like radiogenic and stable-isotope values indicate that they are near-primary magmas supplied to the volcanic front in western Java[7,8].

Inclusions of mafic glass are common in olivine phenocrysts of the high-Mg basalts, and are trapped samples of pre-eruptive melts. Other included phases are Cr-spinel and Al-enstatite (which is rare). These glass inclusions are generally smaller than 50 μm in diameter, and each contains a single vapour bubble decorated with tiny Fe-sulphide blebs; most glass inclusions also contain a single grain of Cr-spinel. Olivine phenocrysts that host glass inclusions are weakly zoned in their interiors and have compositions in the range $Fo_{89–73}$, although most are $>Fo_{83}$ and have NiO contents of 0.31–0.10 wt%. Glass inclusions from two high-Mg basaltic bombs were analysed for major-element, trace-element and volatile contents.

Inclusion glasses range continuously from transitional basaltic to strongly undersaturated compositions with low $SiO_2$ contents, high CaO contents, and high $CaO/Al_2O_3$ ratios, but with alkali contents similar to the transitional basaltic inclusions (Table 1). Glass inclusions have lower MgO contents and Mg/(Mg + Fe) than the host high-Mg basalts, due in part to 5–13 wt% post-entrapment crystallization of olivine on the inclusion walls. Projected from olivine (Fig. 1), to factor out the effects of host-olivine crystallization, the inclusion glasses form an array from near the Galunggung high-Mg basalts (basaltic inclusions) to the diopside–Ca-tschermak–jadeite compositional plane (strongly undersaturated

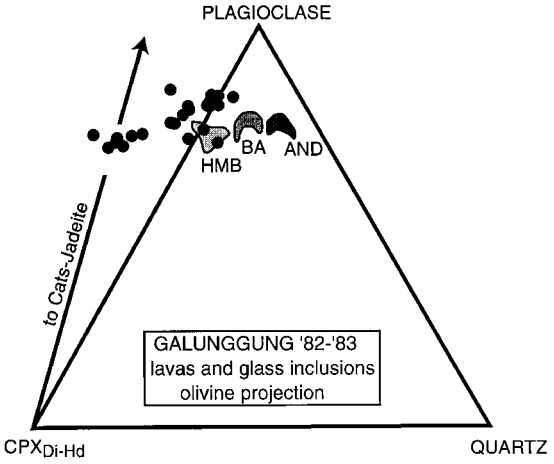


**Figure 1** Galunggung 1982–83 eruption whole rocks (fields) (ref. 7 and this work) and high-Mg-basalt inclusion glasses (filled circles) projected[24] from olivine onto the plagioclase-clinopyroxene (cpx)-quartz compositional plane. Late-erupted high-Mg basalts (HMB), light shading; basaltic andesites (BA), medium shading; and early-erupted andesites (AND), dark shading. $CPX_{Di-Hd}$ is diopside + hedenbergite; arrow shows trajectory to calcium-tschesmak (cats) and jadeite pyroxene components. Whole-rock compositions were measured by X-ray fluorescence at the University of Canterbury, NZ. Glass and mineral inclusions and phenocrysts were analysed by electron-microprobe at the USGS, Menlo Park, CA.